JOC Article

Biosynthesis of the 3,4-Dihydroxybenzoate Moieties of Petrobactin by *Bacillus anthracis*

Andrew T. Koppisch,*[,†,‡] Kinya Hotta,[§] David T. Fox,[†] Christy E. Ruggiero,[†] Chu-Young Kim,[§] Timothy Sanchez,[†] Srinivas Iyer,[†] Cindy C. Browder,[‡] Pat J. Unkefer,[†] and Clifford J. Unkefer*[,†]

Bioscience Division, Los Alamos National Laboratory, Los Alamos, New Mexico 87545, Departments of Chemistry and Biology, Northern Arizona University, Flagstaff, Arizona 86011, and Department of Biological Science, Faculty of Science, National University of Singapore, Singapore 117543

koppisch@lanl.gov; cju@lanl.gov

Received February 21, 2008

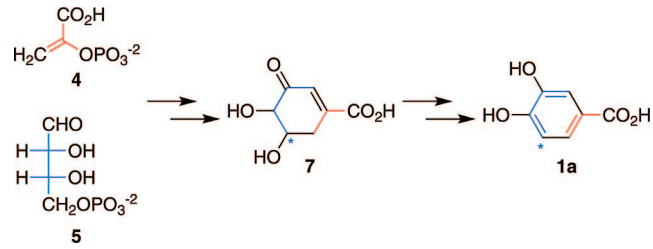

The biosynthesis of the 3,4-dihydroxybenzoate moieties of the siderophore petrobactin, produced by *B. anthracis* str. Sterne, was probed by isotopic feeding experiments in iron-deficient media with a mixture of unlabeled and D-[$^{13}C_6$]glucose at a ratio of 5:1 (w/w). After isolation of the labeled siderophore, analysis of the isotopomers was conducted via one-dimensional ^{1}H and ^{13}C NMR spectroscopy, as well as $^{13}C-^{13}C$ DQFCOSY spectroscopy. Isotopic enrichment and $^{13}C-^{13}C$ coupling constants in the aromatic ring of the isolated siderophore suggested the predominant route for the construction of the carbon backbone of 3,4-DHB (**1**) involved phosphoenol pyruvate and erythrose-4-phosphate as ultimate precursors. This observation is consistent with that expected if the shikimate pathway is involved in the biosynthesis of these moieties. Enrichment attributable to phosphoenol pyruvate precursors was observed at C1 and C6 of the aromatic ring, as well as into the carboxylate group, while scrambling of the label into C2 was not. This pattern suggests **1** was biosynthesized from early intermediates of the shikimate pathway and not through later shikimate intermediates or aromatic amino acid precursors.

Introduction

Bacillus anthracis is a Gram-positive pathogen responsible for the anthrax disease and is of particular concern due to its potential for use as a bioweapon. The spores of *B. anthracis* germinate and replicate within a mammalian host, and upon entry into the bloodstream, rapid growth of the organism ultimately leads to sepsis and death within a matter of days.[1] Iron is a requisite mineral for the proliferation of *B. anthracis*, as well as other pathogens; however, iron homeostasis within a mammalian host is tightly regulated.[2] A common strategy employed by bacteria to solubilize and sequester iron is the biosynthesis and secretion of small molecule high-affinity iron chelators termed siderophores. Siderophore biosynthesis is recognized as a determinant of virulence in many pathogenic bacteria, including *B. anthracis*,[3−5] and inhibitors of siderophore biosynthesis have shown promise as antibiotics against other pathogenic bacteria.[6]

[†] Los Alamos National Laboratory.
[‡] Northern Arizona University.
[§] National University of Singapore.

(1) Koehler, T., M. *Gram-Positive Pathogens*; ASM Press: Washington, DC, 2000; p 519−528.

(2) Griffiths, E. *Iron in Biological Systems*, 2nd ed.; John Wiley & Sons: Chichester, U.K., 1999; p 1−26.

(3) De Voss, J. J.; Rutter, K.; Schroeder, B. G.; Su, H.; Zhu, Y.; Barry, C. E., 3rd. The salicylate-derived mycobactin siderophores of *Mycobacterium tuberculosis* are essential for growth in macrophages. *Proc. Natl. Acad. Sci. U.S.A.* **2000**, *97* (3), 1252–1257.

(4) Cendrowski, S.; MacArthur, W.; Hanna, P. *Bacillus anthracis* requires siderophore biosynthesis for growth in macrophages and mouse virulence. *Mol. Microbiol.* **2004**, *51* (2), 407–417.

(5) Dale, S. E.; Doherty-Kirby, A.; Lajoie, G.; Heinrichs, D. E. Role of siderophore biosynthesis in virulence of *Staphylococcus aureus*: identification and characterization of genes involved in production of a siderophore. *Infect. Immun.* **2004**, *72* (1), 29–37.

10.1021/jo800427f CCC: $40.75
Published on Web 06/27/2008

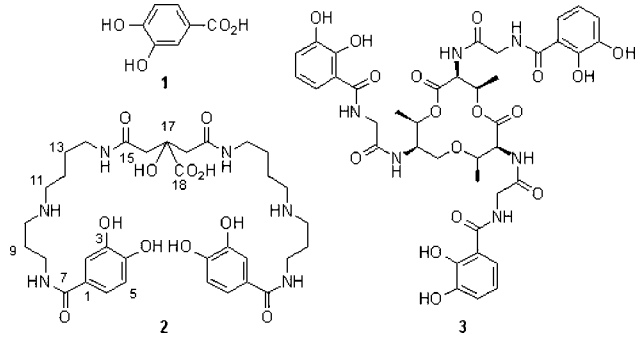

FIGURE 1. Chemical structures of 3,4-DHB (**1**), petrobactin (**2**), and bacillibactin (**3**).

Bacillus anthracis produces two known siderophores, petrobactin (**2**) and bacillibactin (**3**) (Figure 1).[7,8] Unlike **3**, the biosynthesis of **2** is required for *B. anthracis* virulence in a mouse model.[4] Additionally, **3** also differs from **2** in that its production is repressed when grown under conditions that mimic the circulatory system.[7,9] A recent report also observed that **2** is capable of avoiding sequestration by siderocalin, which is a siderophore-binding protein in the human immune system.[10] Therefore, it is generally believed that **2** plays a critical role in the onset of anthrax in a mammalian host, and inhibitors that target its biosynthesis are expected to be effective antibiotics against *B. anthracis*.

Both siderophores produced by *B. anthracis* contain catechol iron-liganding groups; however, the dihydroxybenzoate functional groups found in **2** and **3** are constitutional isomers of one another. This is an important distinction since **2** and a sulfonated derivative are the only characterized siderophores with a 3,4-dihydroxylation pattern in the DHB moiety.[11–14] All other known catecholate containing siderophores have a 2,3-hydroxylation pattern.[15] Since the catecholate groups of this siderophore are the primary sites of iron binding, it is expected that inhibitors of the biosynthesis of **1** will also prevent production of the siderophore that contains them. Additionally, these inhibitors should not affect 2,3-DHB containing siderophore production in other probiotic bacteria and could potentially act as selective antibiotics toward *B. anthracis*.

Although the genomic sequence of *B. anthracis* str. Sterne is completed,[16] the biosynthetic route to **1** in this organism remains elusive. However, the shikimate biosynthetic pathway is the primary means to synthesize aromatic molecules (including aromatic amino acids) in bacteria, plants, and some fungi. The biosynthesis of 2,3-DHB by some bacteria also uses isochorismate, which is a late stage intermediate of this pathway, as a precursor.[17,18] On the basis of this information, three biosynthetic routes to **1** are possible, each making use of intermediates of the shikimate pathway (Scheme 1).

First, **1** could be constructed via early intermediates of the shikimate biosynthetic pathway such as 3-dehydroshikimic acid (**7**), as is observed for gallic acid in some plants and fungi.[19] This route would entail a net dehydration and aromatization of **7**, and this activity is observed in some bacteria, including those capable of aromatic compound biodegradation such as *Klebsiella pneumoniae*.[20] Second, 4-hydroxybenzoic acid (**9**) is generated in one of the terminal steps in the pathway; oxidation of **9** would lead directly to **1**.[21,22] A third option involves formation of **1** from the catabolism and subsequent oxidation of aromatic amino acids such as phenylalanine or tyrosine, which are biosynthesized through the shikimate pathway in the absence of exogenous supplementation. Production of **1** as an intermediate of L-tyrosine catabolism occurs in some fungi,[23] as well as prokaryotes capable of transforming L-tyrosine into coumarate.[24] Further biological precedence for this transformation exists in dopamine biosynthesis, wherein L-tyrosine is oxidized to L-Dopa, which contains a 3,4-dihydroxylated aromatic moiety.[25,26] Given these possibilities, the primary pathway to **1** should be discernible by heavy-atom incorporation using a correlated labeling experiment[27] by adding a mixture of unlabeled and D-[$^{13}C_6$]glucose as the primary carbon source.[16] Glucose is metabolized by *B. anthracis* using the Embden−Meyerhof pathway, which provides intracellular pools of phosphoenol

(6) Ferreras, J. A. R., J. S.; Di Lello, F.; Tan, D. S.; Quadri, L. E. N. Small molecule inhibition of siderophore biosynthesis in *Mycobacterium tuberculosis* and *Yersinia pestis*. *Nat. Chem. Biol.* **2005**, *1* (1), 29–32.

(7) Koppisch, A. T.; Browder, C. C.; Moe, A. L.; Shelley, J. T.; Kinkel, B. A.; Hersman, L. E.; Iyer, S.; Ruggiero, C. E. Petrobactin is the primary siderophore synthesized by *Bacillus anthracis* str. Sterne under conditions of iron starvation. *Biometals* **2005**, *18* (6), 577–585.

(8) Wilson, M. K.; Abergel, R. J.; Raymond, K. N.; Arceneaux, J. E.; Byers, B. R. Siderophores of *Bacillus anthracis, Bacillus cereus*, and *Bacillus thuringiensis*. *Biochem. Biophys. Res. Commun.* **2006**, *348* (1), 320–325.

(9) Garner, B. L.; Arceneaux, J. E.; Byers, B. R. Temperature control of a 3,4-dihydroxybenzoate (protocatechuate)-based siderophore in *Bacillus anthracis*. *Curr. Microbiol.* **2004**, *49* (2), 89–94.

(10) Abergel, R. J.; Wilson, M. K.; Arceneaux, J. E.; Hoette, T. M.; Strong, R. K.; Byers, B. R.; Raymond, K. N. Anthrax pathogen evades the mammalian immune system through stealth siderophore production. *Proc. Natl. Acad. Sci. U.S.A.* **2006**, *103*, 18499–18503.

(11) Barbeau, K.; Zhang, G.; Live, D. H.; Butler, A. Petrobactin, a photoreactive siderophore produced by the oil-degrading marine bacterium *Marinobacter hydrocarbonoclasticus*. *J. Am. Chem. Soc.* **2002**, *124* (3), 378–379.

(12) Bergeron, R. J. H., G.; Smith, R. E.; Bharti, N.; McManis, J. S.; Butler, A. Total synthesis and structure revision of petrobactin. *Tetrahedron* **2003**, *59*, 2007–2014.

(13) Gardner, R. A.; Kinkade, R.; Wang, C.; Phanstiel, O. t. Total synthesis of petrobactin and its homologues as potential growth stimuli for *Marinobacter hydrocarbonoclasticus*, an oil-degrading bacteria. *J. Org. Chem.* **2004**, *69* (10), 3530–3537.

(14) Hickford, S. J.; Kupper, F. C.; Zhang, G.; Carrano, C. J.; Blunt, J. W.; Butler, A. Petrobactin sulfonate, a new siderophore produced by the marine bacterium Marinobacter hydrocarbonoclasticus. *J. Nat. Prod.* **2004**, *67* (11), 1897–1899.

(15) Neilands, J. Siderophores: Structure and function of microbial iron transport compounds. *J. Biol. Chem.* **1995**, *270*, 26723.

(16) Brettin, T. S.; Bruce, D.; Challacombe, J. F.; Gilna, P.; Han, C.; Hill, K.; Hitchcock, P.; Jackson, P.; Keim, P.; Longmire, J.; Lucas, S.; Okinaka, R.; Richardson, P.; Rubin, E.; and Tice, H. Direct submission to NCBI, 2004.

(17) May, J. J.; Wendrich, T. M.; Marahiel, M. A. The dhb operon of *Bacillus subtilis* encodes the biosynthetic template for the catecholic siderophore 2,3-dihydroxybenzoate-glycine-threonine trimeric ester bacillibactin. *J. Biol. Chem.* **2001**, *276* (10), 7209–7217.

(18) Balado, M.; Osorio, C. R.; Lemos, M. L. A gene cluster involved in the biosynthesis of vanchrobactin, a chromosome-encoded siderophore produced by *Vibrio anguillarum*. *Microbiology* **2006**, *152*, 3517–3528.

(19) Werner, I.; Bacher, A.; Eisenreich, W. Retrobiosynthetic NMR studies with 13C-labeled glucose. Formation of gallic acid in plants and fungi. *J. Biol. Chem.* **1997**, *272* (41), 25474–25482.

(20) Li, W.; Xie, D.; Frost, J. W. Benzene-free synthesis of catechol: interfacing microbial and chemical catalysis. *J. Am. Chem. Soc.* **2005**, *127*, 2874–2882.

(21) Entsch, B.; Cole, L. J.; Ballou, D. P. Protein dynamics and electrostatics in the function of *p*-hydroxybenzoate hydroxylase. *Arch. Biochem. Biophys.* **2005**, *433*, 297–311.

(22) Gutteridge, S.; Robb, D. The catecholase activity of *Neurospora* tyrosinase. *Eur. J. Biochem.* **1975**, *54*, 107–116.

(23) Sparnins, V. L.; Burbee, D. G.; Dagley, S. Catabolism of L-tyrosine in *Trichosporon cutaneum*. *J. Bacteriol.* **1979**, *138*, 425–430.

(24) Verhoef, S.; Ruijssenaars, H. J.; de Bont, J. A.; Wery, J. Bioproduction of *p*-hydroxybenzoate from renewable feedstock by solvent-tolerant *Pseudomonas putida* S12. *J. Biotechnol.* **2007**, *132*, 49–56.

(25) Haneda, K.; Watanabe, S.; Takeda, P. Synthesis of L-3,4-dihydroxyphenylalanine from L-tyrosine by microorganisms. *App. Microbiol.* **1971**, *22*, 712–722.

(26) Ali, S.; Schultz, J. L.; Haq, I. U. High performance microbiological transformation of L-tyrosine to L-dopa by *Yarrowia lipolytica* NRRL-143. *BMC Biotechnol.* **2007**, *7*, epub Aug 16.

SCHEME 1. Key Biochemical Steps of the Shikimate Pathway and Three Possible Routes to 3,4-Dihydroxybenzoic Acid (1)

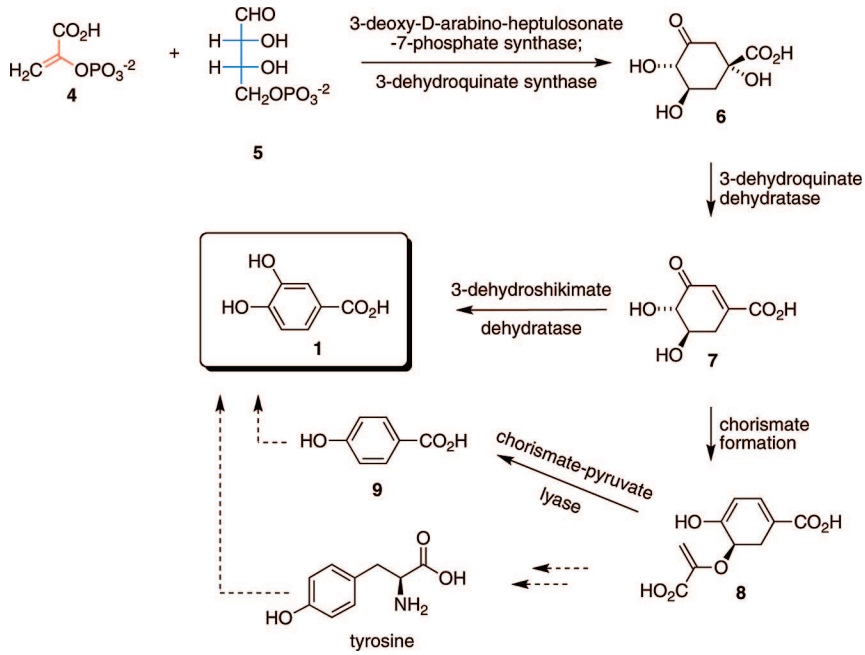

pyruvate (**4**) via conversion of glucose through fructose-6-phosphate. The pentose phosphate pathway is also operable in this organism, and the synthesis of intracellular pools of erythrose-4-phosphate (**5**) originates via the same glucose precursors. Providing 80% unlabeled and 20% D-[$^{13}C_6$]glucose to the organism as the primary carbon source affords fractional enrichment of the pools of both **4** and **5** wherein significant portions of the individual phosphosugars in the pool are either fully labeled with ^{13}C or fully unlabeled. Furthermore, dilution of the label affords a mixture of unique isotopomers of shikimate intermediates that are enriched via a singular incorporation of either **4**, **5**, or derivatives of these precursors. As a consequence, $^{13}C-^{13}C$ couplings are a particularly useful tool to track the fate of the individual carbon bonds in the requisite shikimate precursors **4** and **5** within a biochemical pathway. As has been previously shown for the biosynthesis of gallic acid, this technique is effective to definitively describe both the involvement and orientation of incorporation of these precursors in the biosynthesis of aromatic moieties of molecules.[19,28]

Results

Bacillus anthracis was grown in 1 L of iron-deficient media containing casamino acids and 0.2% (w/w) glucose (20% D-[$^{13}C_6$]/80% natural abundance glucose) as the primary carbon source. Upon removal of cells, petrobactin was purified from the aqueous phase as previously reported.[7] An additional purification step using size exclusion chromatography (Biogel P2) was employed to remove minor contaminants, particularly any **2** present in the iron-chelated form. ^{13}C NMR chemical shifts were consistent with previous reports;[7,12–14] however due to ^{13}C enrichment, complex splitting in the DHB and citrate moieties of **2** is observed as a result of carbon−carbon coupling (Table 1). Incorporation of ^{13}C into the siderophore was verified via HRMS, as numerous isotopomers of **2** were observed in the isolated material.

TABLE 1. Comparison of Observed (D_2O) and Reported ^{13}C NMR Shifts for Labeled 2

position	δC observed (ppm)	multiplicity	δC reported (ppm)[12]
1	125.6	dd (^1J = 62, 57 Hz)	125.4
2	115.8	d (^1J = 73 Hz)	115.0
3	144.0	dd (^1J = 72, 73 Hz)	144.8
4	148.2	dd (^1J = 71, 70 Hz)	148.5
5	115.1, 115.9	d (^1J = 69 Hz), s	114.8
6	120.5	d (^1J = 62 Hz)	118.9
7	170.5	d (^1J = 57 Hz)	166.7
8	36.6	s	36.1
9	25.9	s	26.2
10	45.1	s	44.8
11	47.4	s	46.4
12	23.0	s	23.0
13	25.6	s	26.0
14	38.4	s	37.7
15	172.6	m	169.5
16	44.6	s	43.3
17	75.4	m	73.5
18	178.9	m	175.0

Enrichment of ^{13}C was clearly observed in the dihydroxybenzoate and citrate moieties of **2** in 1-D ^{13}C NMR spectra but not in the spermidine groups. This was attributed to the presence of unlabeled casamino acids in the medium, and spermidine is biosynthesized from lysine. Enrichment was observed at all seven carbon centers of **1**, but the $^1J_{C-C}$ coupling constants indicated that this is primarily due to distinct isotopomers of **1** arising from incorporation of [U-$^{13}C_3$]**4** or [U-$^{13}C_4$]**5**, respectively. C1 of **1** was observed at 125.5 ppm as a doublet of doublets with scalar coupling constants of 62 and 57 Hz, respectively. These coupling constants were consistent with those observed for the doublet attributed to both the carboxylate (170.5 ppm) and C6 (120.5 ppm) (J_{COOH-1} = 57 Hz and J_{6-1} = 62 Hz, respectively). A geminal coupling constant of 3 Hz ($^2J_{6\text{-}COOH}$ and $^2J_{COOH-6}$) was also observed for the carboxylate and

(27) Gould, S. J.; Cane, D. E. Biosynthesis of streptonigrin from [U-13C]-D-glucose. Origin of the quinoline quinone. *J. Am. Chem. Soc.* **1982**, *104*, 343–346.

(28) Werner, R. A.; Rossmann, A.; Schwarz, C.; Bacher, A.; Schmidt, H. L.; Eisenreich, W. Biosynthesis of gallic acid in *Rhus typhina*: discrimination between alternative pathways from natural oxygen isotope abundance. *Phytochemistry* **2004**, *65* (20), 2809–2813.

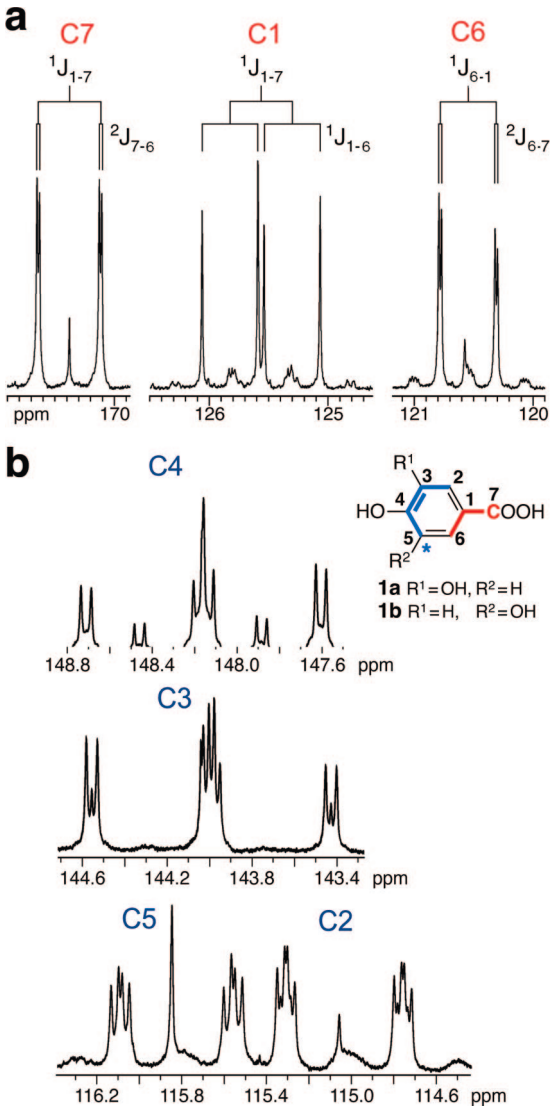

FIGURE 2. (a) 1D-^{13}C spectrum of selected resonances of **1** in isolated isotopomers, with coupling constants identified for the carboxylate carbon (C7), C1, and C2. (b) 1D-^{13}C spectrum of selected resonances of **1** in isolated isotopomers. Carbons pertaining to **4** are colored red, and those pertaining to **5** are blue, with an asterisk delineating potential C1 of **5**.

C6, which is attributed to long-range coupling of these carbons (Figure 2a). We observe a mixture of isotopomers as a result of scrambling of label via intermediary metabolism (Table 2). As is observed in the biosynthesis of gallic acid, major isotopomers of **1** arise from isotopomers of **4** and **5**, respectively. In particular, significant intracellular portions of **5** may exist in unlabeled [U-$^{13}C_4$] (through pentose phosphate pathway). Futile glycolytic/glucogenetic cycling via reversible action of transaldolase will yield D-[1,2,3-$^{13}C_3$]- and D-[4,5,6-$^{13}C_3$]hexoses.[19] Conversion of these hexoses through the pentose pathway will yield 1-^{13}C or 2,3,4-$^{13}C_3$ isotopomers of **5**, respectively. Evidence of isotopomers of **1** attributable to incorporation of [U-$^{13}C_4$]**5** and [2,3,4-$^{13}C_3$]**5** are seen in the resonance for C4 (Figure 2b). Splitting arising from incorporation of [U-$^{13}C_4$] is visible as a doublet of doublets (resonances at 147.6, 148.1, and 148.7 ppm; $^1J_{4-3} = 76$ Hz and $^1J_{4-5} = 75$ Hz, respectively), with geminal coupling to C2 ($^2J_{4-2} = 7$ Hz). A doublet attributable to incorporation of [2,3,4-$^{13}C_3$]**5** is also observed ($^1J_{4-3} = 76$ Hz and $^2J_{4-2} = 7$ Hz). These splitting patterns are

TABLE 2. Isotopomer Analysis[a]

isotopomer **1a**	predominate precursor isotopomers		^{13}C-resonance integrated	fractional intensity
	4[b]	**5**[b]		
[1,6,7-$^{13}C_3$]	[1,2,3-$^{13}C_3$]	N. A.	C1	0.82
[$^{13}C_7$]	[1,2,3-$^{13}C_3$]	[1,2,3,4-$^{13}C_4$]	C1	0.18
[2,3,4,5-$^{13}C_4$]	N. A.	[1,2,3,4-$^{13}C_4$]	C2	0.75
[$^{13}C_7$]	[1,2,3-$^{13}C_3$]	[1,2,3,4-$^{13}C_4$]	C2	0.19
[2-^{13}C]	N. A.	[4-^{13}C]	C2	0.05
[2,3,4,5-$^{13}C_4$]	N. A.	[1,2,3,4-$^{13}C_4$]	C3	1.0
[2,3,4,5-$^{13}C_4$]	N. A.	[1,2,3,4-$^{13}C_4$]	C4	0.83
[2,3,4-$^{13}C_3$]	N. A.	[2,3,4-$^{13}C_3$]	C4	0.17
[2,3,4,5-$^{13}C_4$]	N. A.	[1,2,3,4-$^{13}C_4$]	C5	0.69
[$^{13}C_7$]	[1,2,3-$^{13}C_3$]	[1,2,3,4-$^{13}C_4$]	C5	0.17
[5-^{13}C]	N. A.	[1-^{13}C]	C5	0.14
[1,6,7-$^{13}C_3$]	[1,2,3-$^{13}C_3$]	N. A.	C6	0.76
[$^{13}C_7$]	[1,2,3-$^{13}C_3$]	[1,2,3,4-$^{13}C_4$]	C6	0.19
[6-^{13}C]	[3-^{13}C]	N. A.	C6	0.04
[1,6,7-$^{13}C_3$]	[1,2,3-$^{13}C_3$]	N. A.	C7	1.0

[a] The ratio of isotopomers (derived from **4** and **5**) observable in each center is as expected from supplementation with 20% D-[U-$^{13}C_6$]glucose and 80% natural abundance D-glucose and indicates that there was not significant dilution of the pools of **4** and **5** by carbon from unlabeled amino acids added to the growth medium. In addition, the integrated intensity of the C2, C5, and C6 protonated carbons with shorter T_1 are equal indicating that the pools of **4** and **5** were labeled equivalently. [b] N.A. = natural abundance

consistent with both predicted and observed resonance patterns arising from isotopomers formed by incorporation of [U-$^{13}C_4$]**5** and [2,3,4-$^{13}C_3$]**5** into C4 of gallic acid.[19] Extensive geminal coupling in all aromatic resonances was observed, which is also consistent with previous studies. The singlet observed at 115.9 ppm in C5 was attributed to an isotopomer of **1** that is singly labeled at C5 via incorporation of [1-^{13}C]**5**. Isotopic dilution of labeled three-carbon sugar monomers into fructose-1,6-diphosphate occurs via the reversible action of transaldolase on this substrate and leads to C1 labeled **5**. Observation of this singlet suggests that C1 of **5** corresponds to C5 of **1**. A smaller, broad singlet was also observed at C2. From the 1D spectrum alone, we could not determine if this singlet was also the result of incorporation of C1 labeled **5** or was the result of other mechanisms of isotopic scrambling from glucose, such as futile glycolytic/glyconeogenic cycling or mannitol cycling.[19] The small, broad triplet observable in C6 and quartet observed at C1 are attributable to the predicted fraction of the $^{13}C_7$-isotopomer that would result from condensing [U-$^{13}C_3$]**4** and [U-$^{13}C_4$]**5** using 20% labeling. The small singlets observed at C7 and C6 result from the incorporation of [1-^{13}C]**4** or [3-^{13}C]**4**, which we attribute to the incorporation of [U-$^{13}C_2$]acetate into the TCA cycle via citrate synthase or incorporation of $^{13}CO_2$ into TCA intermediate via PEP carboxykinase. Forward and reverse scrambling through the TCA intermediates would yield [1-^{13}C]- and [3-^{13}C]oxaloacetic acid, which could be decarboxylated to [1-^{13}C]**4** or [3-^{13}C]**4** by PEP carboxykinase.

A two-dimensional ^{13}C−^{13}C DQFCOSY experiment was conducted on the isolated **2**. As shown in Figure 3, correlation was clearly observed between the carboxylate carbon and C1 and C6 of the aromatic ring. Correlation was also observed between C2, C3, C4, and C5; however it was not observed between C1 and C2, which is to be expected if incorporation of **4** and **5** into **1** occurs without involving a symmetrical intermediate.

Observation of this enrichment pattern of **4** into **1** suggests that the primary biosynthetic route does not involve any

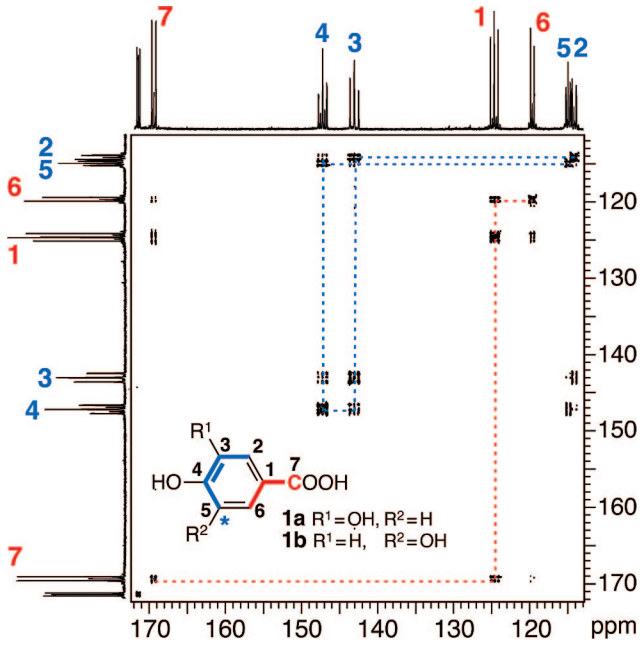

FIGURE 3. 2D $^{13}C-^{13}C$ DQFCOSY spectrum of **1** in isolated isotopomers.

symmetrical intermediates such as those found in the later stages of the shikimate pathway. Thus, biosynthesis through early shikimate intermediates such as **7** is favored over a mechanism involving late intermediates or aromatic amino acids. Further support of this was observed in samples of *B. anthracis* grown in the presence of the inhibitor glyphosate, which inhibits conversion of **12** to **13**.[29] Although bacterial growth was slightly attenuated in the presence of glyphosate, production of **2** remained constant. Additionally, enrichment at the carboxylate carbon itself indicates **1** was not primarily synthesized via conversion of aromatic amino acids, as this label is lost in the shikimate-based synthesis of these molecules. Similarly, the observation of label in the aromatic carbons itself suggests that aromatic amino acids, or derivatives of amino acids, are unlikely contributors to the biosynthesis of **1**, as our growth media contains millimolar concentrations of unlabeled aromatic amino acids (via casamino acids).

Discussion

Since metabolism of the glucose mixture (via glycolysis) initially provides intracellular pools of both unlabeled and fully labeled **4**, this technique provided a means to assess not only incorporation of ^{13}C atoms but also the fate of the individual monomers of **4** upon construction of the **1** moieties. In this strategy, all of the possible routes to **1** yield unique isotopomers. Most significantly, biosynthesis from early shikimate intermediates preserves the regiochemistry of isotopic enrichment initially established by the action of 3-hydroxyquinate synthase, whereas biosynthesis from late shikimate intermediates or aromatic amino acids do not (Scheme 2).

Both formation of **9** from **8** and decarboxylation of **14** afford symmetrical compounds. When **1** is formed via further oxidation of these species, it necessarily provides a mixture of isotopomers enriched in the aromatic ring at either C1 and C2 (**1b**) or C1 and C6 (**1a**). We clearly observe enrichment only at C1 and C6 (**1a**), which indicates synthesis from early shikimate intermediates is the predominant route. Although it is conceivable that other pathways may contribute to intracellular pools of **1**, our experiments indicate these are likely minor contributions. In addition to the evidence provided by our NMR experiments, glyphosate inhibition has little effect on the production of **2**, which further suggests biosynthesis of **1** from a tyrosine precursor is unlikely.

A likely pathway for formation of **1** is via dehydration of **7** through an enzyme with 3-dehydroshikimate dehydratase (DHS) activity[30] to form **15**, which is then expected to rapidly tautomerize to **1**. This is the primary route of formation of **1** in some species of fungi and bacteria,[31–33] and a pathway through this intermediate would be expected to provide the isotopomers we observe in this report (Scheme 3).

No obvious DHS homologues exist in any sequenced *Bacillus* strains, however. If an enzyme with this activity exists in *B. anthracis* Sterne, it likely has little sequence homology to characterized enzymes of this sort. It is worth noting that the protein encoded by *asbF*, which is a gene located in the biosynthetic cluster for the synthesis of **2**, does have structural homology to known DHS enzymes and may be responsible for the synthesis of the catecholate moieties of **2**. Production of **1** has been observed by several *B. anthracis* strains containing *asbF*,[8,9] and we have also observed UV absorbances consistent with a synthetic standard of **1** in dilute acid hydrolysates of **2** isolated from strains of *B. anthracis*, *B. cereus*, and *B. thuringiensis*. Furthermore, the growth of a *B. anthracis* str. Sterne *asbF* deletion strain is impaired relative to the wild-type when both are cultured in an iron-deficient medium, but growth is restored to rates comparable to those of the wild-type when supplemented with exogenous petrobactin.[34] We observe a distinct increase in absorbance at 290 nm when buffered aqueous solutions of **7** are incubated with purified recombinant AsbF, while no increase is noted in the absence of added enzyme.[35] Kinetic studies of the conversion of **7** to **1** by AsbF will be reported elsewhere.

Experimental Section

Bacterial Strains and Growth Conditions. All growths and manipulations of *B. anthracis* Sterne were performed in a certified biosafety level 2 (BSL-2) laboratory using appropriate protective equipment and following the guidelines set forth by the U.S. Centers of Disease Control (CDC) regarding microbiological techniques and decontamination protocols (http://www.cdc.gov/od/ohs/biosfty/bmbl/section3.htm#Biosafety%202). Starter cultures of *B. anthracis*

(29) Moore, B. S.; Floss, H. G. Biosynthetic studies on the origin of the cyclohexanecarboxylic acid moiety of Ansatrienin A and *o*-cyclohexyl fatty acids. *J. Nat. Prod.* **1994**, *57*, 382–386.

(30) Stroman, P.; Reinert, W. R.; Giles, N. H. Purification and characterization of 3-dehydroshikimate dehydratase, an enzyme in the inducible quinic acid catabolic pathway of *Neurospora crassa*. *J. Biol. Chem.* **1978**, *253*, 4593–4598.

(31) Wheeler, K. A.; Lamb, H. K.; Hawkins, A. R. Control of metabolic flux through the quinate pathway in *Aspergillus nidulans*. *Biochem. J.* **1996**, *315*, 195–205.

(32) Elsemore, D. A.; Ornston, L. N. Unusual ancestry of dehydratases associated with quinate catabolism in *Acinetobacter calcoaceticus*. *J. Bacteriol.* **1995**, *177*, 5971–5978.

(33) Adachi, O.; Tanasupawat, S.; Yoshihara, N.; Toyama, H.; Matsushita, H. 3-Dehydroquinate production by oxidative fermentation and further conversion of 3-dehydroquinate to the intermediates in the shikimate pathway. *Biosci. Biotechnol. Biochem.* **2003**, *67*, 2124–2131.

(34) Lee, J. Y.; Janes, B. K.; Passalacqua, K. D.; Pfleger, B. F.; Bergman, N. H.; Liu, H.; Hakansson, K.; Somu, R. V.; Aldrich, C. C.; Cendrowski, S.; Hanna, P. C.; Sherman, D. H. Biosynthetic analysis of the petrobactin siderophore pathway from *Bacillus anthracis*. *J. Bacteriol.* **2007**, *189* (5), 1698–710.

(35) Rotenberg, S. L.; Sprinson, D. B. Isotope effects in 3-dehydroquinate synthase and dehydratase. Mechanistic implications. *J. Biol. Chem.* **1978**, *253*, 2210–2215.

SCHEME 2. Establishment of Regiochemistry of Isotopic Enrichment by the Action of 3-Hydroxyquinate Synthase and the Fate of the Enriched Atoms in 10 by the Action of the Three Potential Synthetic Routes to 1[a]

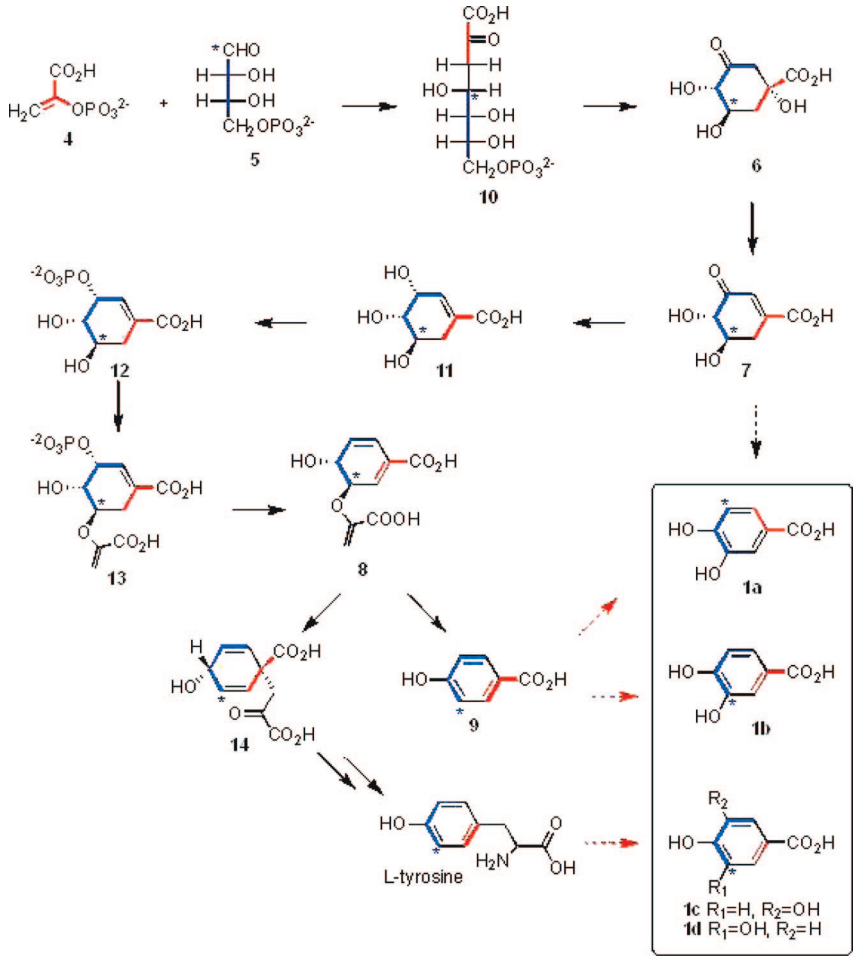

[a] The black arrow indicates the predominant pathway suggested by our results. The carbon labeled with an asterisk signifies C1 of **5**.

SCHEME 3. Fate of Isotopically Enriched Atoms of 7 Predicted by the Mechanism of Action of Dehydroshikimate Dehydratase Enzymes

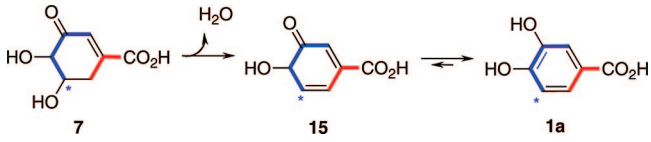

Sterne were made by inoculating a single colony from a nutrient agar plate into 25 mL of iron-free media. Upon observing confluent growth, one 25 mL subculture was used to inoculate 2 L of the same media in 4 L baffled flasks, and the cultures were covered in foil and shaken (120 rpm) at room temperature in ambient air for 12−24 h. In this study, a total volume 6 L was grown. After growth was completed, the solution was sterilized by being passed through a 0.22 μm filter.

Purification of Petrobactin. XAD-2 resin (15 g/L) was added to filtered media and stirred for 12 h. The resin was then loaded into a column and washed with ddH_2O, until the eluent showed a minimal absorbance at 260 nM. Crude petrobactin was then eluted from the column with 25% methanol. The presence of petrobactin and other iron-binding species was also tracked by analyzing eluted fractions with the Chrome-azurol S (CAS) assay.[36] The methanol in the eluent was removed with a rotary evaporator, and the sample was then reduced to dryness via lyophilization to yield approximately 10 mg of a yellow-brown powder. The crude material was then redissolved in a minimal amount of ddH_2O and minor contaminants were removed by passing the material over a Biogel P2 fine column. The petrobactin was eluted from the Biogel column (1 mL/h) in this same solvent. The eluent was monitored at 260 nM and with the CAS assay, and fractions containing siderophore were lyophilized to dryness to afford petrobactin (8 mg) as a white powder: ^{13}C NMR (125 MHz, D_2O) δ 178.9,172.6, 148.2, 144.0, 125.6, 120.5, 115.8, 115.1, 75.4, 47.4, 45.1, 44.6, 38.4, 36.6, 25.9, 25.6, 23.0. UV (H_2O, pH = 3) 230 (30,100 M^{-1} cm^{-1}), 257 (10,200 M^{-1} cm^{-1}), 291 (5400 M^{-1} cm^{-1}). HRMS *m/z* calcd for $C_{34}H_{51}N_6O_{11}$ $(M + H)^+$ 719.3610, found 719.3688.

Bacterial Culture in the Presence of Glyphosate. Culture growths were performed in the same manner as reported above, with the following modifications. Glyphosate was added to a final concentration of 6 mM along with Gibco Vitamin Mix (25 μL per 25 mL aliquot of bacterial media). The vitamins were added to offset any disruption of endogenous vitamin biosynthetic pathways in *B. anthracis*.[29] The bacteria were grown at RT for 24 h and the media sterilized by passing through a 0.22 μm filter. Petrobactin was purified as described. Analysis via MALDI-TOF MS was performed on an Applied Biosystems Voyager MS using α-cyano-hydroxycinnamic acid as matrix (0.1−1 to 1:1 sample to matrix ratios) and standard instrument settings.

Acknowledgment. D.T.F. is supported through an Agnew National Security Postdoctoral Fellowship. T.S. is supported via

(36) Schwyn, B.; Neilands, J. B. Universal chemical assay for the detection and determination of siderophores. *Anal. Biochem.* **1987**, *160* (1), 47–56.

the NSF PUSH program for undergraduate students in northern New Mexico. We thank Drs. Suraj Dhungana, Hakim Boukhalfa, and Ryszard Michalsyk for helpful discussions.

Supporting Information Available: 1D ^{13}C spectra of the isolated isotopomers, HRMS data of the isotopomers as well as HRMS of **2** isolated from cells grown in unenriched medium for comparison, and a timecourse of UV absorbance at 290 of incubations of **7** with recombinant AsbF. This material is available free of charge via the Internet at http://pubs.acs.org.

JO800427F